Springer

Journal of Mechanical Science and Technology 23 (2009) 2444~2455

Journal of Mechanical Science and Technology

www.springerlink.com/content/1738-494x
DOI 10.1007/s12206-009-0708-6

Two-fluid non-Newtonian models for blood flow in catheterized arteries - A comparative study †

D. S. Sankar[1] and Usik Lee[2,*]

[1]*School of Mathematical Sciences, University Science Malaysia, 11800 Penang, Malaysia*
[2]*Department of Mechanical Engineering, Inha University, 253 Yonghyun-Dong, Nam-Gu, Incheon 402-751, Republic of Korea*

(Manuscript Received November 28, 2008; Revised July 1, 2009; Accepted July 3, 2009)

Abstract

Steady flow of blood through catheterized arteries is studied by assuming the blood as a two-fluid model with the suspension of all the erythrocytes in the core region as a non-Newtonian fluid and the plasma in the peripheral layer as a Newtonian fluid. The non-Newtonian fluid in the core region of the artery is modeled as (i) Casson fluid and (ii) Herschel-Bulkley fluid. The expressions for the shear stress, velocity, flow rate, wall shear stress and flow resistance, obtained by Sankar and Lee (2008a, 2008b) for the two-fluid Casson model and two-fluid Herschel-Bulkley model are used to get the data for comparison. It is noticed that the plug flow velocity, velocity distribution and flow rate for the two-fluid H-B model are considerably higher than that of the two-fluid Casson model for a given set of values of the parameters. Further, it is found that the resistance to flow is significantly lower for the two-fluid H-B model than that of the two-fluid Casson model. Thus, the two-fluid H-B model is more useful than the two-fluid Casson model to analyze the blood flow through catheterized arteries.

Keywords: Two-fluid models; Newtonian fluid; Casson fluid; Herschel-Bulkley fluid; Steady flow; Catheterized arteries

1. Introduction

Catheters have many applications in contemporary medical science, and several types of catheters are used in clinics for the measurement of various physiologically important flow quantities. The measurement of the flow quantities (such as arterial blood pressure, flow velocity and flow rate) as well as the diagnosis and treatment of various arterial diseases (such as X-ray angiography, intravascular ultrasound and coronary balloon angioplasty) is done through an appropriate catheter-tool device by inserting the device into an artery and positioning it in the desired part of the arterial network [1]. Catheters are even used to clear the short occlusions from the walls of a stenosed artery. The insertion of a catheter in an artery will alter the flow field, modify the pressure distribution and hence increase the flow resistance. Thus, the pressure or pressure gradient recorded by a transducer attached to the catheter will differ from that of an uncatheterized artery and hence, it is essential to know the catheter induced error [2]. Even a very small angioplasty guidewire leads to a sizable increase in flow resistance. For an angioplasty guidewire, over the range of catheter radius ratio (ratio of catheter radius to coronary vessel radius) from 0.3 to 0.7 (which is currently used clinically), even for Newtonian fluid, the flow resistance increases by a large factor of 3-33 for concentric configurations [3]. For smaller infusion catheter, the increase in flow resistance is less, although still appreciable. Hence, it is meaningful to study the increase in flow resistance due to catheterization.

Several theoretical and experimental investigations are done to analyze the blood flow through catheterized arteries [1-6]. MacDonald [7] analyzed the blood

† This paper was recommended for publication in revised form by Associate Editor Haecheon Choi
*Corresponding author. Tel.: +82 32 860 7318, Fax.: +82 32 866 1434
E-mail address: ulee@inha.ac.kr

flow characteristics in catheterized arteries using conformal transformation and finite difference method. The effect of catheterization on various flow characteristics in a curved artery was analyzed by Karahalios [8] and Jayaraman and Tiwari [9]. Daripa and Dash [1] have studied the blood flow characteristics in an eccentric catheterized artery using a fast algorithm. In all the above investigations, blood was treated as a Newtonian fluid. But it is well known that blood, being a suspension of cells, behaves like a non-Newtonian fluid at low shear rate $(\dot{\gamma} < 10/\sec)$ and during its flow through narrow blood vessels of diameter 0.02 - 5 *mm* [10-14].

Chakravarthy et al. [15] and Misra and Pandey [16] have pointed out that for blood flowing through narrow blood vessels, there is a peripheral layer of plasma and a core region of suspension of all the erythrocytes. Hence, for a more realistic description of blood flow, it is appropriate to treat the blood as a two-fluid model consisting of a core region containing all the erythrocytes as a non-Newtonian fluid and the plasma in the peripheral layer as a Newtonian fluid [17-19]. Sankar and Lee [20, 21] have analyzed two-phase fluid models for blood flow through narrow arteries at low shear rates, by treating the fluid in the core region as (i) Casson model and (ii) Herschel-Bulkley (H-B) model, respectively. In both two-fluid models, the fluid in the peripheral layer is treated as Newtonian fluid.

It is noticed that blood obeys Casson's equation only for moderate shear rate and the Herschel-Bulkley equation represents fairly closely what is occurring in blood [22]. Chaturani et al. [13] have mentioned that for tube diameter 0.095*mm* blood behaves like Herschel–Bulkley fluid rather than power law and Bingham fluids. Iida [23] reports, "The velocity profiles in the arterioles having diameter less than 0.1*mm* are generally explained fairly by the two models. However, velocity profiles in the arterioles whose diameters are less than 0.065*mm* do not conform to the Casson model but can still be explained by the H–B fluid model. Moreover, the H-B fluid model can be reduced to the power law fluid model when the yield stress is zero and Bingham fluid model when its power law index n takes the value 1, so that the two-fluid power law and Bingham models can be studied from the two-fluid H-B model itself as its particular cases. Thus, the two-fluid H-B model is more suitable than the two-fluid Casson model to the studies of blood flow through catheterized arteries. Hence, in this paper, we have compared the effect of various parameters on the flow quantities of the two-fluid H-B model and two-fluid Casson model and brought out the advantages of two-fluid H-B model over the two-fluid Casson model for the flow of blood through catheterized arteries. The governing equations and the boundary conditions of both the two-fluid models, and the expressions obtained for the various flow quantities of these models by Sankar and Lee [20, 21] are mentioned in brief in this study and are used to perform a comparative study.

To idealize the present model to the mathematical modeling, the segment of the arterial wall is treated as rigid, neglecting the permeability of the arterial wall, and the catheter is assumed to be inserted co-axially though it is inserted eccentrically into the artery in some cases, depending on the usage of the catheter. The segment of the artery under study is assumed to be non-tapered and non-stenotic. Further, the flow in the artery is assumed to be laminar, axially symmetric, pulsatile and fully developed, though the flow may be underdeveloped, unsteady, turbulent and asymmetric if the catheter is inserted into an artery with considerable angle of tapering and severe stenosis. The maximum diameter of the narrow arteries which are considered in this study is restricted to 5 *mm* [14]. The maximum diameter of the catheters which are considered in this study is restricted to 2.6 *mm* [3]. The layout of the paper is as follows.

The formulation and method of solution of (i) two-phase Casson fluid model and (ii) two-phase Herschel-Bulkley (H-B) fluid model are briefly given in section 2. The variations of the flow quantities of these two-fluid models on the yield stress, catheter radius ratio and peripheral layer thickness are analyzed in section 3. The increase in the flow resistance due to catheterization for different types of catheters which are used in clinics is also given for both the two-phase fluid models and are analyzed in section 3. The results are summarized and the advantages of two-fluid H-B model over the two-fluid Casson are mentioned in the concluding section 4.

2. Mathematical formulation

Consider an axially symmetric, laminar, steady and fully developed flow of blood (assumed to be incompressible) in an artery in which a catheter is introduced coaxially, where the artery is modeled as a rigid walled circular tube of radius $\bar{R}$. The catheter

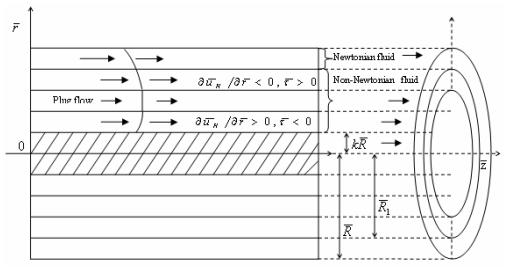

Fig. 1. Geometry of the catheterized artery modeled as two-fluid non-Newtonian model.

radius is taken to be $k\bar{R}\ (k<1)$. Blood is treated as a two-fluid model with the suspension of all the erythrocytes in the core region as a non-Newtonian fluid and the plasma in the peripheral region as a Newtonian fluid. The non-Newtonian fluid in the core region is represented by (i) Casson fluid model and (ii) Herschel-Bulkley fluid model. We have used the cylindrical polar coordinates $(\bar{r},\bar{\phi},\bar{z})$, where $\bar{r}$ and $\bar{z}$ denote the radial and axial coordinates and $\bar{\phi}$ is the azimuthal angle. The flow geometry of the two-fluid non-Newtonian model for blood flow through catheterized artery is shown in Fig. 1.

2.1 Two-fluid Casson model

2.1.1 Governing equations and boundary conditions

It can be shown that the radial velocity is negligibly small in magnitude and may be neglected for low Reynolds number flow and the pressure gradient is a function of $\bar{z}$ alone. The simplified form of the momentum equations of the flow are

$$\frac{d\bar{p}}{d\bar{z}}=-\frac{1}{\bar{r}}\frac{d}{d\bar{r}}\left(\bar{r}\,\bar{\tau}_C\right) \quad \text{in} \quad k\bar{R}\le\bar{r}\le\bar{R}_1 \tag{1}$$

$$\frac{d\bar{p}}{d\bar{z}}=-\frac{1}{\bar{r}}\frac{d}{d\bar{r}}\left(\bar{r}\,\bar{\tau}_N\right) \quad \text{in} \quad \bar{R}_1\le\bar{r}\le\bar{R} \tag{2}$$

where $\bar{p}$ denotes the pressure and $\bar{\tau}_C$ and $\bar{\tau}_N$ denote the shear stress of the Casson fluid and Newtonian fluid, respectively, and $\bar{R}_1$ is the radius of the core region of the artery. The simplified form of the constitutive equations of the fluid in motion in the core region (Casson fluid) and peripheral layer (Newtonian fluid) are given by

$$\bar{\mu}_C\frac{\partial\bar{u}_C}{\partial\bar{r}}=\left|\bar{\tau}_C\right|\left(1-\frac{2\sqrt{\bar{\tau}_y}}{\sqrt{\left|\bar{\tau}_C\right|}}+\frac{\bar{\tau}_y}{\left|\bar{\tau}_C\right|}\right) \tag{3}$$

$$\text{for}\ \frac{\partial\bar{u}_C}{\partial\bar{r}}>0 \text{ and } \bar{\tau}_C<0 \quad \text{and} \quad k\bar{R}\le\bar{r}\le\lambda_1\bar{R}$$

$$\frac{\partial\bar{u}_C}{\partial\bar{r}}=0 \quad \text{if} \quad \left|\bar{\tau}_C\right|\le\bar{\tau}_y \ \text{ and } \ \lambda_1\bar{R}\le\bar{r}\le\lambda_2\bar{R} \tag{4}$$

$$\bar{\mu}_C\frac{\partial\bar{u}_C}{\partial\bar{r}}=-\left|\bar{\tau}_C\right|\left(1-\frac{2\sqrt{\bar{\tau}_y}}{\sqrt{\left|\bar{\tau}_C\right|}}+\frac{\bar{\tau}_y}{\left|\bar{\tau}_C\right|}\right)$$

$$\text{for}\ \frac{\partial\bar{u}_C}{\partial\bar{r}}<0 \ \text{ and } \ \bar{\tau}_C>0 \quad \text{and} \quad \lambda_2\bar{R}\le\bar{r}\le\lambda_1\bar{R} \tag{5}$$

$$\bar{\mu}_N\frac{\partial\bar{u}_N}{\partial\bar{r}}=-\left|\bar{\tau}_N\right| \quad \text{for} \quad \frac{\partial\bar{u}_N}{\partial\bar{r}}<0 \text{ and } \bar{\tau}_N>0 \quad \text{and} \quad \bar{R}_1\le\bar{r}\le\bar{R} \tag{6}$$

where $\bar{u}_C$, $\bar{u}_N$ are the axial component of the fluid's velocity in the core region and peripheral region, respectively; $\bar{\mu}_C$, $\bar{\mu}_N$ are the viscosities of the Casson fluid and Newtonian fluid, respectively; $\bar{\tau}_y$ is the yield stress; λ_1 and λ_2 are the yield planes bounding the plug flow region. Eqs. (1), (2) and (3)- (6) can be solved with the help of the following boundary conditions.

$$\bar{u}_C=0 \ \textit{at} \ \ \bar{r}=k\bar{R} \ \text{ and } \ \bar{u}_N=0 \ \text{ at } \ r=\bar{R} \tag{7}$$

$$\bar{u}_C=\bar{u}_N \ \text{ and } \ \bar{\tau}_C=\bar{\tau}_N \ \text{ at } \ \bar{r}=\bar{R}_1 \tag{8}$$

2.1.2 Method of solution

Let $\bar{p}_0$ be the absolute magnitude of the typical pressure gradient. Let us introduce the following non-dimensional variables:

$$\begin{aligned}
&u_C=\bar{u}_C\big/\left(\bar{p}_0\bar{R}^2/2\bar{\mu}_C\right),\ \ u_N=\bar{u}_N\big/\left(\bar{p}_0\bar{R}^2/2\bar{\mu}_N\right),\\
&r=\bar{r}/\bar{R},\ R_1=\bar{R}_1/\bar{R},\\
&z=\bar{z}/\bar{R},\ \ \tau_C=\bar{\tau}_C\big/\left(\bar{p}_0\bar{R}/2\right),\ \ \ \tau_N=\bar{\tau}_N\big/\left(\bar{p}_0\bar{R}/2\right),\\
&\theta=\bar{\tau}_y\big/\left(\bar{p}_0\bar{R}/2\right)
\end{aligned} \tag{9}$$

where θ is the non-dimensional yield stress. Since, the flow is assumed as steady, the pressure gradient can be written as

$$\frac{d\bar{p}}{d\bar{z}}=-\bar{p}_0P \tag{10}$$

where P is the non-dimensional steady state pressure gradient. Using Eqs. (9) and (10), the momentum Eqs. (1) and (2) reduced, respectively, to

$$2P = \frac{1}{r}\frac{d}{dr}(r\tau_C) \quad \text{if} \quad k \le r \le R_1 \tag{11}$$

$$2P = \frac{1}{r}\frac{d}{dr}(r\tau_N) \quad \text{if} \quad R_1 \le r \le 1 \tag{12}$$

Similarly, using Eqs. (9) and (10), the constitutive Eqs. (3)-(6) are simplified, respectively, to

$$\frac{du_C}{dr} = |\tau_C|\left(1 - \frac{2\sqrt{\theta}}{\sqrt{|\tau_C|}} + \frac{\theta}{|\tau_C|}\right) \quad \text{if} \quad \frac{du_C}{dr} > 0 \ \text{and} \ \tau_C < 0 \ \text{and} \ k \le r \le \lambda_1 \tag{13}$$

$$\frac{du_C}{dr} = -|\tau_C|\left(1 - \frac{2\sqrt{\theta}}{\sqrt{|\tau_C|}} + \frac{\theta}{|\tau_C|}\right) \quad \text{if} \quad \frac{du_C}{dr} < 0 \ \text{and} \ \tau_C > 0 \ \text{and} \ \lambda_2 \le r \le R_1 \tag{14}$$

$$\frac{du_C}{dr} = 0 \quad \text{if} \quad \tau_C \le \theta \ \text{and} \ \lambda_1 \le r \le \lambda_2 \tag{15}$$

$$\frac{du_N}{dr} = -|\tau_N| \quad \text{for} \quad \frac{du_N}{dr} < 0 \ \text{and} \ \tau_N > 0 \ \text{and} \ R_1 \le r \le 1 \tag{16}$$

The boundary conditions (in the non-dimensional form) are

$$u_C = 0 \ \text{at} \ r = k \ \text{and} \ u_N = 0 \ \text{at} \ r = 1 \tag{17}$$

$$u_C = u_N \ \text{and} \ \tau_C = \tau_N \ \text{at} \ r = R_1 \tag{18}$$

From Eqs. (13)- (16) and Fig. 1, it is clear that the flow in $k \le r \le 1$ is a four region one, in which the core region has a flat velocity profile and hence forms the plug flow region. For mathematical representation, let this plug flow region be defined by $\lambda_1 \le r \le \lambda_2$, where $k \le \lambda_1, \lambda_2 \le 1$. Here, λ_1 and λ_2 are the unknown constants to be determined. From the continuity of the shear stress along the boundary of the plug flow region, we have

$$-\tau_C\big|_{r=\lambda_1} = \theta = \tau_C\big|_{r=\lambda_2} \tag{19}$$

Solving Eqs. (11)-(16), one can obtain the following expressions for the shear stress and velocity distribution in the core region and the peripheral region.

$$\tau_C = (P/r)\left(r^2 - \lambda^2\right) \tag{20}$$

$$\tau_N = (P/r)\left(r^2 - \lambda^2\right) \tag{21}$$

$$u_C^{+}(r) = P\left[\lambda^2 \log\left(\frac{r}{k}\right) - \frac{1}{2}\left(r^2 - k^2\right) + \beta(r-k) - 2\sqrt{\beta}\int_k^r \sqrt{\frac{\lambda^2 - r^2}{r}}\, dr\right]$$

when $k \le r \le \lambda_1$ (22)

$$u_p = \text{constant when} \quad \lambda_1 \le r \le \lambda_2 \tag{23}$$

$$u_C^{++}(r) = P\left[\frac{1}{2}\left(1 - r^2\right) + \lambda^2 \log r + \beta(R_1 - r) - 2\sqrt{\beta}\int_r^{R_1} \sqrt{\frac{r^2 - \lambda^2}{r}}\, dr\right] \text{ when}$$

$\lambda_2 \le r \le R_1$ (24)

$$u_N = (P/2)\left[1 - r^2 + 2\lambda^2 \log(r)\right] \text{ when } R_1 \le r \le 1 \tag{25}$$

where u_p denotes the plug flow velocity, u_C^{+} and u_C^{++} are the fluid's velocity in the regions $k \le r \le \lambda_1$ and $\lambda_2 \le r \le R_1$ respectively, $\lambda^2 = \lambda_1\lambda_2$ and $\lambda_2 - \lambda_1 = (\theta/P) = \beta$. The details of obtaining Eqs. (20)-(25) are given in Sankar and Lee [20]. By the continuity of the velocity distribution throughout the flow field, we have the condition

$$u_C^{+}(r = \lambda_1) = u_p = u_C^{++}(r = \lambda_2) \tag{26}$$

Substitution of Eqs. (22) and (24) in Eq. (26) gives

$$\left(1 + \lambda_1^2 - \lambda_2^2 - k^2\right) + 2\lambda^2 \log\left(k\lambda_2/\lambda_1\right) + 2\beta\left(R_1 - \lambda_1 - \lambda_2 + k\right) + 4\sqrt{\beta}\left[\int_k^{\lambda_1} \sqrt{\frac{\lambda^2 - r^2}{r}}\, dr - \int_{\lambda_2}^{R_1} \sqrt{\frac{r^2 - \lambda^2}{r}}\, dr\right] = 0 \tag{27}$$

Using $\lambda^2 = \lambda_1\lambda_2$ and $\lambda_2 - \lambda_1 = (\theta/P) = \beta$ in Eq. (27), we get

$$3\beta^2 + 6\beta\lambda_1 - \left(1 - k^2\right) - 2\beta\left(R_1 + k\right) - 2\lambda_1\left(\lambda_1 + \beta\right)\log\left(k\left(\lambda_1 + \beta\right)/\lambda_1\right) - 4\sqrt{\beta}\left[\int_k^{\lambda_1} \sqrt{\frac{\lambda_1\left(\lambda_1 + \beta\right) - r^2}{r}}\, dr - \int_{\lambda_1+\beta}^{R_1} \sqrt{\frac{r^2 - \lambda_1\left(\lambda_1 + \beta\right)}{r}}\, dr\right] = 0 \tag{28}$$

Eq. (28) is solved numerically for λ_1 using Regula-Falsi method; the integrals are evaluated numerically using Simpson's rule. Once λ_1 is known, λ_2 is determined by using $\lambda_2 - \lambda_1 = (\theta/P) = \beta$. The

steady flow rate Q is given by

$$\begin{aligned} Q &= 8\int_k^1 u\, r\, dr \\ &= P\left\{\left(1-k^2\right)\left(1+k^2-2\lambda^2\right)+\left(\lambda_1-\lambda_2\right)^3\left(\lambda_1+\lambda_2\right)\right. \\ &\quad +\frac{4}{3}\beta\left(R_1^3-\lambda_1^3-\lambda_2^3+k^3\right) \\ &\quad \left.+8\sqrt{\beta}\left[\int_k^{\lambda_1}\sqrt{\frac{\lambda^2-r^2}{r}}\; r^2\, dr-\int_{\lambda_2}^{R_1}\sqrt{\frac{r^2-\lambda^2}{r}}\; r^2\, dr\right]\right\} \end{aligned} \tag{29}$$

The details of obtaining the flow rate are given in Sankar and Lee [20]. The wall shear stress in the artery can be obtained from Eq. (21) and is given by

$$\tau_w = \tau_N\big|_{r=1} = P\left(1-\lambda^2\right) \tag{30}$$

The resistance to flow per unit length of the artery is given by

$$\Lambda = \left(P/Q\right) \tag{31}$$

When $R_1 = 1$, the present model reduces to the single-fluid Casson model, and in such a case the expressions for velocity, flow rate, wall shear stress and frictional resistance are in good agreement with those of Dash et al. [11].

2.2 Two-fluid herschel-bulkley model

2.2.1 Governing equations and boundary conditions

The basic momentum equations in this case simplified to

$$\begin{aligned} \frac{d\bar{p}}{d\bar{z}} &= -\frac{1}{\bar{r}}\frac{d}{d\bar{r}}\left(\bar{r}\,\bar{\tau}_H\right) \quad \text{in} \quad k\bar{R} \le \bar{r} \le \bar{R}_1 \\ \frac{d\bar{p}}{d\bar{z}} &= -\frac{1}{\bar{r}}\frac{d}{d\bar{r}}\left(\bar{r}\,\bar{\tau}_N\right) \quad \text{in} \quad \bar{R}_1 \le \bar{r} \le \bar{R} \end{aligned} \tag{32}$$

where $\bar{p}$ denotes the pressure and $\bar{\tau}_H$ and $\bar{\tau}_N$ denote the shear stress of the Herschel-Bulkley fluid and Newtonian fluid, respectively. The simplified forms of the constitutive equation of the fluids in motion in the core region (Herschel-Bulkley fluid) and peripheral layer (Newtonian fluid) are given by

$$\bar{\mu}_H\frac{d\bar{u}_H}{d\bar{r}} = \left|\bar{\tau}_H\right|^n\left(1-\frac{n\bar{\tau}_y}{\left|\bar{\tau}_H\right|}\right) \quad \text{if} \quad \frac{d\bar{u}_H}{d\bar{r}} > 0 \;\; \text{and} \;\; \bar{\tau}_H < 0 \;\; \text{and} \;\; k\bar{R} \le \bar{r} \le \lambda_1\bar{R} \tag{33}$$

$$\frac{\partial\bar{u}_H}{\partial\bar{r}} = 0 \quad \text{if} \quad \bar{\tau}_H \le \bar{\tau}_y \;\; \text{and} \;\; \lambda_1\bar{R} \le \bar{r} \le \lambda_2\bar{R} \tag{34}$$

$$\bar{\mu}_H\frac{d\bar{u}_H}{d\bar{r}} = -\left|\bar{\tau}_H\right|^n\left(1-\frac{n\bar{\tau}_y}{\left|\bar{\tau}_H\right|}\right) \quad \text{if} \quad \frac{d\bar{u}_H}{d\bar{r}} < 0 \;\; \text{and} \;\; \bar{\tau}_H > 0 \;\; \text{and} \;\; \lambda_2\bar{R} \le \bar{r} \le \bar{R}_1 \tag{35}$$

$$\bar{\mu}_N\frac{\partial\bar{u}_N}{\partial\bar{r}} = -\left|\bar{\tau}_N\right| \quad \text{for} \quad \frac{\partial\bar{u}_N}{\partial\bar{r}} < 0 \;\; \text{and} \;\; \bar{\tau}_N > 0 \;\; \text{and} \;\; \bar{R}_1 \le \bar{r} \le \bar{R} \tag{36}$$

where $\bar{u}_H$, $\bar{u}_N$ are the axial component of the fluid's velocity in the core region and peripheral region; $\bar{\mu}_H$, $\bar{\mu}_N$ are the viscosities of the Herschel-Bulkley fluid and Newtonian fluid; $\bar{\tau}_y$ is the yield stress; λ_1 and λ_2 are the yield planes bounding the plug flow region. Eqs. (31) - (36) can be solved with the help of the following boundary conditions.

$$\bar{u}_H = 0 \;\; \text{at} \;\; \bar{r} = k\bar{R} \;\; \text{and} \;\; \bar{u}_N = 0 \;\; \text{at} \;\; r = \bar{R} \tag{37}$$

$$\bar{u}_H = \bar{u}_N \;\; \text{and} \;\; \bar{\tau}_H = \bar{\tau}_N \;\; \text{at} \;\; \bar{r} = \bar{R}_1 \tag{38}$$

2.2.2 Method of solution

Let $\bar{p}_0$ be the absolute magnitude of the typical pressure gradient. Let us introduce the following non-dimensional variables:

$$\begin{aligned} &u_H = \bar{u}_H/\left(\bar{p}_0\bar{R}^2/2\bar{\mu}_0\right), \;\; u_N = \bar{u}_N/\left(\bar{p}_0\bar{R}^2/2\bar{\mu}_N\right), \\ &r = \bar{r}/\bar{R}, \; R_1 = \bar{R}_1/\bar{R}, \;\; z = \bar{z}/\bar{R}, \\ &\tau_H = \bar{\tau}_H/\left(\bar{p}_0\bar{R}/2\right), \; \tau_N = \bar{\tau}_N/\left(\bar{p}_0\bar{R}/2\right), \; \theta = \bar{\tau}_y/\left(\bar{p}_0\bar{R}/2\right) \end{aligned} \tag{39}$$

where $\bar{\mu}_0 = \bar{\mu}_H\left(2/\bar{p}_0\bar{R}\right)^{n-1}$ is the typical viscosity coefficient having the dimension as that of the Newtonian fluid's viscosity and θ is the non-dimensional yield stress. Since, the flow is assumed as steady, the pressure gradient can be written as

$$\frac{d\bar{p}}{d\bar{z}} = -\bar{p}_0 P \tag{40}$$

where P is the non-dimensional steady state pressure gradient. Using Eqs. (39) and (40), the momentum Eqs. (31) and (32) reduced to

$$2P = \frac{1}{r}\frac{d}{dr}\left(r\tau_H\right) \quad \text{if} \quad k \le r \le R_1 \tag{41}$$

$$2P = \frac{1}{r}\frac{d}{dr}\left(r\tau_N\right) \quad \text{if} \quad R_1 \le r \le 1 \tag{42}$$

Similarly, using Eqs. (39) and (40), the constitutive Eqs. (33)-(36) are simplified to

$$\frac{du_H}{dr} = |\tau_H|^n \left(1 - \frac{n\theta}{|\tau_H|}\right) \quad \text{if } \frac{du_H}{dr} > 0 \text{ and } \tau_H < 0 \text{ and } k \le r \le \lambda_1 \tag{43}$$

$$\frac{du_H}{dr} = -|\tau_H|^n \left(1 - \frac{n\theta}{|\tau_H|}\right) \quad \text{if } \frac{du_H}{dr} < 0 \text{ and } \tau_H > 0 \text{ and } \lambda_2 \le r \le R_1 \tag{44}$$

$$\frac{du_H}{dr} = 0 \quad \text{if} \quad \tau_H \le \theta \text{ and } \lambda_1 \le r \le \lambda_2 \tag{45}$$

$$\frac{du_N}{dr} = -|\tau_N| \quad \text{for } \frac{\partial u_N}{\partial r} < 0 \text{ and } \tau_N > 0 \text{ and } R_1 \le r \le 1 \tag{46}$$

The boundary conditions (in the non-dimensional form) are

$$u_H = 0 \quad at \quad r = k \quad and \quad u_N = 0 \quad at \quad r = 1 \tag{47}$$

$$u_H = u_N \quad and \quad \tau_H = \tau_N \quad at \quad r = R_1 \tag{48}$$

From the continuity of the shear stress along the boundary of the plug flow region, we have

$$-\tau_H\big|_{r=\lambda_1} = \theta = \tau_H\big|_{r=\lambda_2} \tag{49}$$

Solving Eqs. (41)-(46) with the help of the boundary conditions (47)-(49), one can get the following expressions for the shear stress and velocity of the fluids in the core region and peripheral region.

$$\tau_H = (P/r)\left(r^2 - \lambda^2\right) \tag{50}$$

$$\tau_N = (P/r)\left(r^2 - \lambda^2\right) \tag{51}$$

$$u_H^+(r) = P^n \left[\int_k^r \left(\frac{\lambda^2 - r^2}{r}\right)^n dr - n\beta \int_k^r \left(\frac{\lambda^2 - r^2}{r}\right)^{n-1} dr\right]$$

when $k \le r \le \lambda_1$ (52)

u_p = constant when $\lambda_1 \le r \le \lambda_2$ (53)

$$u_H^{++}(r) = (P/2)\left[1 - R_1^2 + 2\lambda^2 \log(R_1)\right] + p^n \left[\int_r^{R_1} \left(\frac{r^2 - \lambda^2}{r}\right)^n dr - n\beta \int_r^{R_1} \left(\frac{r^2 - \lambda^2}{r}\right)^{n-1} dr\right] \text{ when}$$

$\lambda_2 \le r \le R_1$ (54)

$$u_N = (P/2)\left[1 - r^2 + 2\lambda^2 \log(r)\right]$$

when $R_1 \le r \le 1$ (55)

where u_p denotes the plug flow velocity, u_H^+ and u_H^{++} are the fluid's velocity in the regions $k \le r \le \lambda_1$ and $\lambda_2 \le r \le R_1$ respectively. The details for obtaining Eqs. (50) – (55) are given in Sankar and Lee [21]. By the continuity of the velocity distribution throughout the flow field:

$$u_H^+(r = \lambda_1) = u_p = u_H^{++}(r = \lambda_2) \tag{56}$$

This gives

$$P^n \left\{\int_k^{\lambda_1} \left(\frac{\lambda^2 - r^2}{r}\right)^n dr - \int_{\lambda_2}^{R_1} \left(\frac{r^2 - \lambda^2}{r}\right)^n dr - n\beta \left[\int_k^{\lambda_1} \left(\frac{\lambda^2 - r^2}{r}\right)^{n-1} dr - \int_{\lambda_2}^{R_1} \left(\frac{r^2 - \lambda^2}{r}\right)^{n-1} dr\right]\right\} - \frac{P}{2}\left[1 - R_1^2 + 2\lambda^2 \log(R_1)\right] = 0 \tag{57}$$

Using Eqs. (27) and (29) in Eq. (36),

$$P^n \left\{\int_k^{\lambda_1} \left(\frac{\lambda_1(\lambda_1 + \beta) - r^2}{r}\right)^n dr - \int_{\lambda_1 + \beta}^{R_1} \left(\frac{r^2 - \lambda_1(\lambda_1 + \beta)}{r}\right)^n dr - n\beta \left[\int_k^{\lambda_1} \left(\frac{\lambda_1(\lambda_1 + \beta) - r^2}{r}\right)^{n-1} dr - \int_{\lambda_1 + \beta}^{R_1} \left(\frac{r^2 - \lambda_1(\lambda_1 + \beta)}{r}\right)^{n-1} dr\right]\right\} - \frac{P}{2}\left[1 - R_1^2 + 2\lambda^2 \log(R_1)\right] = 0 \tag{58}$$

The above equation is solved numerically for λ_1 using Regula–Falsi method; the integrals are evaluated using Trapezoidal rule. Once λ_1 is known, λ_2 is determined from $\lambda_2 - \lambda_1 = (\theta/P) = \beta$. The steady flow rate Q is given by

$$Q = 8\int_k^1 rudr = 4P^n \left\{\left[-\int_k^{\lambda_1} \left(\frac{\lambda^2 - r^2}{r}\right)^n r^2 dr + \int_{\lambda_2}^{R_1} \left(\frac{r^2 - \lambda^2}{r}\right)^n r^2 dr\right] + n\beta \left[\int_k^{\lambda_1} \left(\frac{\lambda^2 - r^2}{r}\right)^{n-1} r^2 dr - \int_{\lambda_2}^{R_1} \left(\frac{r^2 - \lambda^2}{r}\right)^{n-1} r^2 dr\right]\right\} + P\left[\left(1 - R_1^2\right) + 2\left(1 - R_1^4\right) - 2\lambda_2^2\left(1 - R_1^2\right) + 4\lambda^2\left(2R_1^2 - \lambda_2^2\right)\log(R_1)\right] \tag{59}$$

The details for obtaining Eq. (59) are given in Sankar and Lee [21]. The wall shear stress in the artery can be obtained from Eq. (51) and is given by

$$\tau_w = \tau_N\big|_{r=1} = P\left(1-\lambda^2\right) \tag{60}$$

The flow resistance per unit length of the artery is given by

$$\Lambda = \left(P/Q\right) \tag{61}$$

When $R_1 = 1$, the present model reduces to the single fluid model of a Herschel-Bulkley fluid, and in such a case the expressions for velocity, flow rate, wall shear stress and frictional resistance are in good agreement with Sankar and Hemalatha [24].

3. Results and discussion

The objective of the present analysis is to compare and bring out the advantages of the two-fluid Herschel-Bulkley (H-B) model over the two-fluid Casson model. It is generally observed that the typical value of the power law index n of the Herschel-Bulkley fluid for blood flow models is generally taken as 0.95 [24]. The value 0.1 is used for the non-dimensional yield stress θ of two-fluid H-B model and two-fluid Casson model. The range 0 – 0.6 is used for the catheter radius ratio k [11]. The value of the ratio β of the central core radius $\beta\overline{R}_0$ to the normal artery radius $\overline{R}_0$ in the unobstructed artery is taken as 0.95 [16] and the range 0.85–1.0 is used to study the effect of the peripheral layer thickness of the two-fluid models. The value of the steady state pressure gradient P is taken as 1 [20].

3.1 Yield plane locations

The location of a point where the shear stress is equal to the yield stress is called a yield point, and the locus of such points is called yield surface or yield plane. In the case of a tube flow, there is only one yield plane, whereas for annular flow, there are two yield planes $r = \lambda_1$ and $r = \lambda_2$ and these two yield planes form the boundary of the plug flow region. It is noted that β ($= \lambda_2 - \lambda_1$) is the width of the plug flow region. For steady flow, the yield plane locations do not change during the course of motion, but they change with respect to the other parameters. The variation of the yield plane locations with the yield stress θ for the two-fluid H-B model and two-fluid Casson model with the catheter radius ratio k = 0.5 and the interface location R_1 = 0.95, is shown in Fig. 2. It is observed that the width of the plug flow region increases with the increase of the yield stress θ for both the two-fluid models. Further, it is noted that for any value of the yield stress, the width of the plug flow region is almost the same for both the two-fluid models.

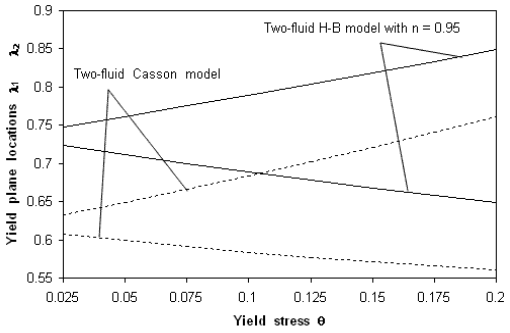

Fig. 2. Variation of yield plane locations with yield stress for two-fluid H-B model and two-fluid Casson model with k = 0.5.

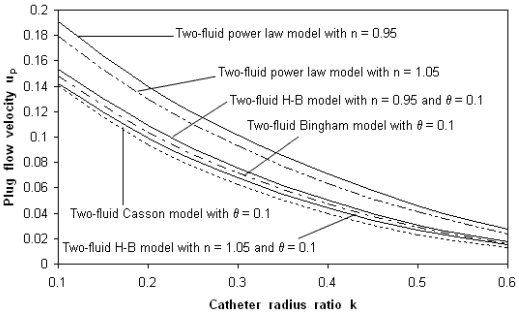

Fig. 3. Variation of plug flow velocity with catheter radius ratio for different two-fluid models with R_1 = 0.95.

3.2 Plug flow velocity

The variation of the plug flow region with catheter radius ratio k for different two-fluid models with interface position R_1 = 0.95 and yield stress θ = 0.1 is depicted in Fig. 3. The plug flow velocity for different two-fluid models decreases nonlinearly with the increase of the catheter radius ratio k. The plug flow velocity decreases rapidly as the catheter radius ratio k increases from 0.1 to 0.4, and then it decreases slowly as the catheter radius ratio increases further from 0.4 to 0.6. For a given value of the catheter radius ratio k, the plug flow velocity is maximum for the two-fluid power law model and minimum for the

two-fluid Casson model. The plug flow velocity for the two-fluid H-B model is higher than that of the two-fluid Casson model. The plug flow velocity decreases with the increase of the power law index n. Fig. 3 shows the simultaneous effects of the non-Newtonian nature of the fluid and the catheter radius ratio k on different two-fluid models for blood flow through catheterized arteries.

3.3 Velocity distribution

The velocity distribution for different two-fluid models and single-fluid models with yield stress θ = 0.1, catheter radius ratio k = 0.5 and interface position R_1 = 0.95, is depicted in Fig. 4. One can notice the flattened velocity profiles for the two-fluid models, which have fluids with yield stress in the core region, and the usual parabolic velocity profile for the two-fluid power model, which has no yield stress. Among the two-fluid models, the two-fluid power law model has the highest velocity and the two-fluid Casson model has the lowest velocity. The velocities for the two-fluid H-B model and two-fluid Bingham model are lower than those of the two-fluid power law model and higher than those of the two-fluid Casson model. Also, the velocity of the two-fluid H-B model is marginally higher than that of the single-fluid H-B model, and the velocity of the two-fluid Casson model is significantly higher than that of the single-fluid Casson model. The lowest velocity is obtained for the single-fluid Casson model. It is of interest to note that the plot of the single-fluid H-B model is in good agreement with Fig. 4 of Sankar and Hemalatha [24], and the plot of the single-fluid Casson model is in good agreement with Fig. 3 of Dash et al. [11]. Fig. 4 depicts the effects of the non-Newtonian nature of blood on velocity distribution when blood flows through catheterized arteries.

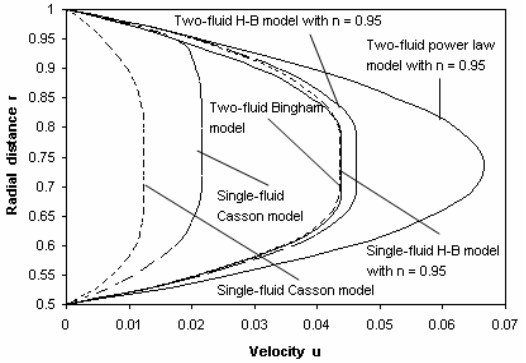

Fig. 4. Velocity distribution for different fluid models with θ = 0.1, k = 0.5 and R_1 = 0.95.

3.4 Flow rate

The variation of the flow rate with interface position R_1 (parameter corresponding to the peripheral layer thickness) for different two-fluid models with catheter radius ratio k = 0.5 is sketched in Fig. 5. The flow rate for all the two-fluid models decreases linearly with the increase of the interface position R_1 (as the peripheral layer thickness decreases). At any location of the interface R_1, the flow rate is maximum for the two-fluid power law model and minimum for the two-fluid Casson model. For a given value of the interface location, the flow rate for the two-fluid H-B model is higher than that of the two-fluid Casson model and lower than that of the two-fluid power law model. Also, the flow rate decreases marginally as the power law index n increases from 0.95 to 1.05. The flow rate of the two-fluid Casson model is significantly lower than that of the other two-fluid models. The decrease in the flow rate of the two-fluid Casson model is much slower than that of the other models, when the interface location R_1 increases. Fig. 5 shows the influence of the peripheral layer thickness on the different two-fluid models for the flow of blood through catheterized arteries.

Fig. 6 shows the variation of the flow rate with yield stress for different two-fluid models with catheter radius ratio k = 0.5 and interface location R_1 = 0.95. It is noticed that the flow rate decreases slowly (linearly) with the increase of the yield stress θ for the two-fluid H-B models and two-fluid Bingham model. Also, the flow rate decreases nonlinearly with the increase of the yield stress θ for the two-fluid Casson model; this decrease is quite fast when the yield stress

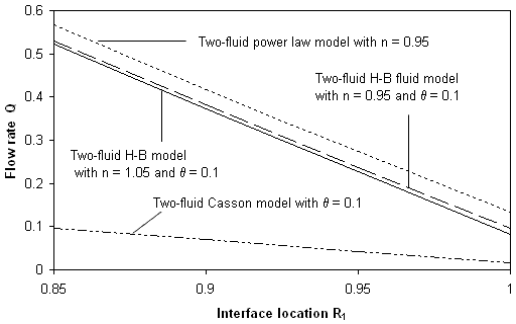

Fig. 5. Variation of flow rate with interface location for different two-fluid models with k = 0.5.

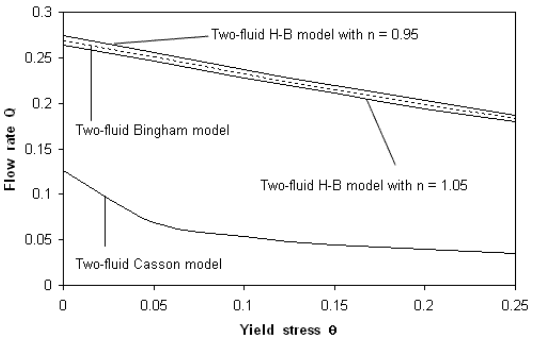

Fig. 6. Variation of flow rate with yield stress for different two-fluid models with $k = 0.5$ and $R_1 = 0.95$.

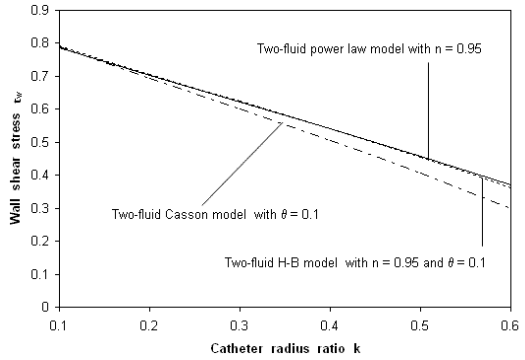

Fig. 7. Variation of wall shear stress with catheter radius ratio for different two-fluid models with $R_1 = 0.95$.

θ increases from 0 to 0.05 and is almost the same constant when the yield stress θ increases further from 0.05 to 0.25. For a given value of the yield stress θ, the flow rates for the two-fluid H-B and Bingham models are considerably higher than that of the two-fluid Casson model. Fig. 6 shows the non-Newtonian effects of the blood when it flows through catheterized arteries.

3.5 Wall shear stress

The variation of the wall shear stress with the catheter radius ratio k for different two-fluid models with $R_1 = 0.95$ is shown in Fig. 7. It is clear that the wall shear stress decreases linearly for all the two-fluid models with the increase of the catheter radius ratio k. For a given value of the catheter radius ratio k, wall shear stress is maximum for the two-fluid power law model and minimum for the two-fluid Casson model, and there is only a marginal difference between the plots of the wall shear stress of the two-fluid power law model and two-fluid H-B model. But,

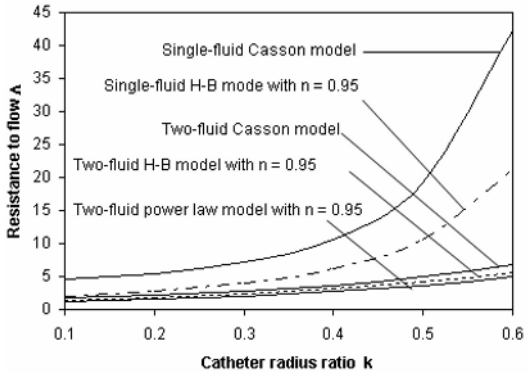

Fig. 8. Variation of resistance to flow with catheter radius ratio for different fluid models with $R_1 = 0.95$ and θ = 0.1.

the difference becomes considerable for the two-fluid Casson model over the other two-fluid models when the catheter radius ratio increases from 0.2 from 0.6. Fig. 7 shows the effects of the catheter on the wall shear stress of the different two-fluid models when blood flows through catheterized arteries.

3.6 Resistance to flow

Fig. 8 depicts the variation of the resistance to flow with catheter radius ratio k for different fluid models with the yield stress θ = 0.1 and the interface position $R_1 = 0.95$. One can observe that for all the two-fluid models, the resistance to flow increases slowly as the catheter radius ratio k increases. It is seen that for the single-fluid H-B model and single-fluid Casson model, the resistance to flow increases slowly (linearly) as the catheter radius ratio k increases form 0.1 to 0.3, and it increases rapidly (nonlinearly) as the catheter radius ratio k increases further from 0.3 to 0.6. For a given value of the catheter radius ratio k, the resistance to flow is maximum for the single-fluid Casson model and is minimum for the two-fluid power law model. The resistance to flow for the two-fluid H-B models is higher than that of the two-fluid power law model and lower than those of the two-fluid Casson model. It is found that the resistance to flow of the single-fluid Casson model and single-fluid H-B model is significantly higher than that of the two-fluid Casson model and two-fluid H-B model, respectively. It is of interest to note that the plot of the single-fluid Casson model is in good agreement with Fig. 12 of Dash et al. [11] and the plot of the single-fluid H-B model is in good agreement with Fig. 10 of Sankar and Hemalatha [24]. Fig. 8 shows the effects

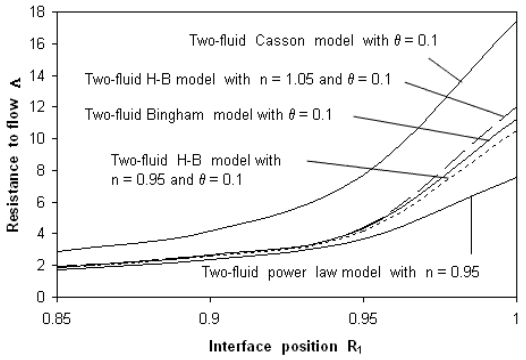

Fig. 9. Variation of resistance to flow with interface position for different two-fluid models with k = 0.5.

of the catheter and the non-Newtonian behavior of blood on the resistance to flow for different two-fluid models.

The variation of the resistance to flow with interface location R_1 for different two-fluid models with catheter radius ratio k = 0.95 is shown in Fig. 9. Note that the resistance to flow increases very slowly with the increase of the interface location R_1 (with the decrease of the peripheral layer thickness) from 0.85 to 0.925, and it increases rapidly (nonlinearly) as the interface location R_1 increases from 0.925 to 1. The behavior of the two-fluid models in this case is the same as that we have observed for them in Fig. 8.

The increase in the frictional resistance due to the catheterization is defined as the ratio between the resistance to flow of a fluid model in a catheterized artery for a given set of values of the parameters and the resistance to flow of the same fluid in the uncatheterized artery for the same set of values of the parameters [24]. The estimates of the increase in the resistance to flow with the increase of the catheter radius ratio k for different values of the yield stress θ for the two-fluid H-B model and two-fluid Casson model with R_1 = 0.95 are given in Table 1. For the range 0.1 - 0.6 of the catheter radius ratio, the range of increase in frictional resistance for the two-fluid H-B model is 1.05-3.31, 1.06-3.57 and 1.08-3.71 when the yield stress θ values are 0.1, 0.15 and 0.2, respectively, and for the two-fluid Casson model, these increases are 1.53-6.16, 1,43-5.58 and 1.45-5.64 when the yield stress θ values are 0.1, 0.15 and 0.2, respectively. It is important to note that the estimates of the increase in the resistance to flow values are considerably much smaller for the two-fluid H-B model than that of the two-fluid Casson model.

Table 1. The estimates of the frictional resistance increase with catheter radius ratio k for different values of the yield stress θ for two-fluid H-B model and two-fluid Casson model with effects on catheterization with R_1 = 0.95.

k	Two-fluid H-B model with n = 0.95			Two-fluid Casson model		
	θ = 0.1	θ = 0.15	θ = 0.2	θ = 0.1	θ = 0.15	θ = 0.2
0.1	1.0494	1.0634	1.0769	1.5336	1.4330	1.4503
0.2	1.1576	1.1902	1.2208	1.9739	1.8573	1.8964
0.3	1.3485	1.4082	1.4621	2.5753	2.4386	2.5067
0.4	1.6728	1.7747	1.8607	3.4255	3.2591	3.3658
0.5	2.2370	2.4082	2.5326	4.6124	4.392	4.5342
0.6	3.3049	3.5664	3.7079	6.1550	5.8200	5.6403

Table 2. Different types of catheters used in cardiovascular treatment, their sizes and the flow quantities measured using them.

Type of catheter	Catheter diameter d_i (*mm*)	Flow quantity measured
Angioplasty catheter guidewire	0.356	Pressure drop
Coronary angioplasty catheter	1.400	Pressure distal to lesion
Guiding catheter	2.600	Pressure at coronary ostium
Doppler catheter	1.000	Velocity proximal to lesion
Coronary infusion catheter	0.660	Pressure drop across lesion

Catheters play an important role in the clinical investigations, since they are used to measure different types of flow quantities. Some types of catheters used in clinics, their sizes and their usage are mentioned in Table 2 [24], where d_i is the diameter of the catheter and d_0 is the diameter of the artery. As a possible application of the present study to the medical field, the different types of the catheters with sizes, which are generally used in the medical field [21], and the corresponding range of estimates of the increase in the frictional resistance for the two-fluid and single-fluid Casson models with θ = 0.1 and R_1 = 0.95 are given in Table 3. It is observed that the range of estimates of the increase in the resistance to flow for the two-fluid H-B model is significantly very small when compared with that of the two-fluid Casson model. Hence, it is strongly felt that the two-fluid H-B model will have more applicability than the two-fluid Casson model in clinical use.

Table 3. Range of frictional resistance increase for different types of catheters for two-fluid H-B model and two-fluid Casson model with $R_1 = 0.95$ and $\theta = 0.1$.

Type of catheter	Range of catheter size d_1/d_0	Two-fluid H-B model with $n = 0.95$	Two-fluid Casson model
Guidewire	0.08-0.18	1.0135-1.0420	1.31-1.50
Infusion	0.14-0.33	1.0289-1.1119	1.42-1.81
Angioplasty catheter	0.3-0.6	1.0950-1.3484	1.74-2.56

The present mathematical model can be used to predict the various flow quantities like pressure, pressure drop and velocity, which are usually measured in clinics with the use of appropriate catheter devices. The present study can be used to predict the pressure in arteries of diameter 3.0 *mm,* which is usually measured in clinics with the use of angioplasty catheter guidewire of diameters 0.356 *mm* and 1.4 *mm* [25]. Further, our study can be used to find the theoretical value of the pressure at a coronary ostium, which is usually measured in medical labs with the help of the guiding catheter of diameter 2.6 *mm* [3]. Our theoretical model can measure the velocity in the arterioles of diameter 2.0 *mm,* which is measured in clinics with the use of Doppler catheter of diameter 1.0 *mm* [26]. Furthermore, the present study can also be used to calculate the pressure drop across a lesion in the arteries of diameter 1.5 *mm,* which is measured in labs by the use of coronary infusion catheter of diameter 0.66 *mm* [27].

4. Conclusions

The steady flow of blood through catheterized arteries is analyzed, assuming blood as a (i) two-fluid Casson model and (ii) two-fluid Herschel-Bulkley model. The effects of the catheterization, non-Newtonian nature of blood and the influence of the peripheral layer thickness on the yield plane locations, velocity, wall shear stress and frictional resistance are analyzed for different two-fluid models. It is found that the width of the plug flow region increases with the increase of the yield stress. The plug flow velocity, velocity distribution and the flow rate for the two-fluid H-B model are considerably higher than that of the two-fluid Casson fluid model for a given set of values of the parameters. Further, the resistance to flow is significantly very low for the two-fluid H-B model than that of the two-fluid Casson model.

Since the difference between the estimates of the two-fluid H-B model and the two-fluid Casson model is substantial, one can expect a marked increase in the velocity and flow rate in the blood flow by modeling the flowing blood as the two-fluid H-B model than as the two-fluid Casson model. The increase in resistance to flow is an important factor in the studies of blood rheology and is considerably low for the two-fluid H-B model; therefore, it is believed that the use of the two-fluid H-B model for analyzing the blood flow may give data that are more reliable. By using the two-fluid H-B model, physicians can be more accurate in predicting the post-catheterization flow quantities. In view of the above discussion, it is concluded that the two-fluid H-B model could be very useful for analyzing the blood flow through catheterized arteries.

References

[1] P. Daripa and R. K. Dash, A numerical study of pulsatile blood flow in an eccentric catheterized artery using a fast algorithm, *Journal Engineering Mathematics* 42 (2002) 1-22.

[2] R. K. Dash, G. Jayaraman and K. N. Metha, Flow in a catheterized curved artery with stenosis, *Journal of Biomechanics* 32 (1999) 49-61.

[3] L. H. Back, Estimated mean flow resistance increase during coronary artery catheterization, *Journal of Biomechanics* 27 (1994) 169-175.

[4] L. H. Back, E. Y. Kwack and M. R. Back, Flow rate-pressure drop relation in coronary angioplasty: Catheter obstruction effect, *ASME Journal of Biomechanical Engineering* 118 (1996) 83-89.

[5] G. Jayaraman and R. K. Dash, Numerical study of flow in a constricted curved annulus: An application to flow in a catheterized artery, *Journal of Engineering Mathematics* 40 (2001) 355-376.

[6] A. Sarkar and G. Jayaraman, Correction to flow rate-pressure drop relation in coronary angioplasty: Steady streaming effect, *Journal of Biomechanics* 31 (1998) 781-791.

[7] D. A. MacDonald, Pulsatile flow in a catheterized artery, *Journal of Biomechanics* 19 (1986) 239-249.

[8] G. T. Karahalios, Some possible effects of a catheter on the arterial wall, *Medical Physics* 17 (1990) 922-925.

[9] G. Jayaraman, and K. Tiwari, Flow in a catheterized curved artery, *Medical and Biological Engineering and Computing* 33 (1995) 1-6.

[10] C. Tu and M. Deville, Pulsatile flow of non-Newtonian fluids through arterial stenosis, *Journal of Biomechanics* 29 (1996) 899-908.

[11] R. K. Dash, G. Jayaraman and K. N. Metha, Estimation of increased flow resistance in a narrow catheterized artery – A theoretical model, *Journal of Biomechanics* 29 (1996) 917-930.

[12] P. Chaturani and R. Ponnalagar Samy, A study of non- Newtonian aspects of blood flow through stenosed arteries and its applications in arterial diseases, Biorheology 22 (1985) 521-531.

[13] P. Chaturani and R. Ponnalagar Samy, Pulsatile flow of a Casson fluid through stenosed arteries with application to blood flow, *Biorheology* 23 (1986) 499-511.

[14] L. H. Back, Estimated mean flow resistance increase during coronary artery catheterization, *Journal of Biomechanics* 27 (1994) 169-175.

[15] S. Chakravarthy, S. Sarifuddin and P.K. Mandal, Unsteady flow of a two-layer blood stream past a tapered flexible artery under stenotic conditions, *Computational Methods in Applied Mathematic*s 4 (2004) 391-409.

[16] J. C. Misra and S. K. Pandey, Peristaltic transport of blood in small vessels: Study of a mathematical model, *Computers and Mathematics with Applications* 43 (2002) 1183-1193.

[17] V. P. Srivastava, and M. Saxena, Two-layered model of Casson fluid flow through stenotic blood vessels: Applications to the cardiovascular system, *Journal of Biomechanics* 27 (1994) 921-928.

[18] J. B. Shukla, R. S. Parihar and S. P. Gupta, Biorheological aspects of blood flow through artery with mild stenosis: Effects of peripheral layer, *Biorheology* 17 (1980) 403-410.

[19] M. Sharan and A.S. Popel, A two-phase model for flow of blood in narrow tunes with increased effective viscosity near the wall, *Biorheology* 28 (2001) 415.

[20] D. S. Sankar and U. Lee, Two-fluid Herschel–Bulkley model for blood flow in catheterized arteries, *Journal of Mechanical Science and Technology* 22 (2008a) 1008-1018.

[21] D. S. Sankar and U. Lee, Two-fluid non-linear model for flow in catheterized blood vessels, *Int. J. Non-Linear Mechanics* 43 (2008b) 622-631.

[22] G. W. Scott Blair and D. C. Spanner, An introduction to Biorheology, Elsevier Scient. Publ. Co., Amsterdam, Oxford and New York (1974).

[23] N. Iida, Influence of plasma layer on steady blood flow in microvessels, *Japanese Journal of Applied Physics* 17 (1978) 203-214.

[24] D. S. Sankar, and K. Hemalatha, A Non-Newtonian fluid flow model for blood flow through a catheterized artery - Steady flow, Applied Mathematical Modeling 31 (2007) 1847 - 1864.

[25] R. F. Wilson, M. R. Johnson, M. L. Marcus, P. E.G. Alyward, D. J. Skorton, S. Collings and C. W. White, The effect of coronary angioplasty on coronary flow reserv, *Circulation* 77 (1988) 873 – 885.

[26] E. L. Johnson, P. G. Yock, V. K. Hargrave, J. P. Srebro, S. M. Manubens, W. Seitz and T. A. Ports, Assessment of severity of coronary stenosis using a Doppler catheter. Validation of a method based on the continuity equation, *Circulation* 80 (1989) 625-635.

[27] P. Ganz, D. P. Harrington, J. Gaspar and W. H. Barry, Phasic pressure gradients across coronary and renal artery stenosis in humans, *Am. Heart J.* 106 (1983) 399-1406.

Dr. D. S. Sankar received his B. Sc degree in Mathematics from the University of Madras, India, in 1989. He then received his M .Sc, M. Phil and Ph.D. degrees from Anna University, India in 1991, 1992 and 2004, respectively. Dr. D. S. Sankar is currently working at the School of Mathematical Sciences, University Science Malaysia, Malaysia. He serves as a referee for several reputed international journals. Dr. D. S. Sankar's research interests include Fluid Dynamics, Hemodynamics, Differential Equations and Numerical Analysis.

Dr. Usik Lee received his B.S. degree in Mechanical Engineering from Yonsei University, Korea in 1979. He then received his M.S. and Ph.D. degrees in Mechanical Engineering from Stanford University, USA in 1982 and 1985, respectively. Dr. Lee is currently a Professor at the Department of Mechanical Engineering at Inha University in Incheon, Korea. He serves as a referee for many reputed international journals. Dr. Lee's research interests include structural dynamics, biomechanics, and computational mechanics.